NASA/TM—2007–215074

Capillary Liquid Acquisition Device Heat Entrapment

L.G. Bolshinskiy
Jacobs Engineering MSFC Group/The University of Alabama in Huntsville, Huntsville, Alabama

L.J. Hastings
Alpha Technology, Inc., Huntsville, Alabama

G. Statham
Jacobs Engineering MSFC Group/ERC Inc., Huntsville, Alabama

J.B. Turpin
Marshall Space Flight Center, Marshall Space Flight Center, Alabama

September 2007

The NASA STI Program…in Profile

Since its founding, NASA has been dedicated to the advancement of aeronautics and space science. The NASA Scientific and Technical Information (STI) Program Office plays a key part in helping NASA maintain this important role.

The NASA STI program operates under the auspices of the Agency Chief Information Officer. It collects, organizes, provides for archiving, and disseminates NASA's STI. The NASA STI program provides access to the NASA Aeronautics and Space Database and its public interface, the NASA Technical Report Server, thus providing one of the largest collections of aeronautical and space science STI in the world. Results are published in both non-NASA channels and by NASA in the NASA STI Report Series, which includes the following report types:

- TECHNICAL PUBLICATION. Reports of completed research or a major significant phase of research that present the results of NASA programs and include extensive data or theoretical analysis. Includes compilations of significant scientific and technical data and information deemed to be of continuing reference value. NASA's counterpart of peer-reviewed formal professional papers but has less stringent limitations on manuscript length and extent of graphic presentations.

- TECHNICAL MEMORANDUM. Scientific and technical findings that are preliminary or of specialized interest, e.g., quick release reports, working papers, and bibliographies that contain minimal annotation. Does not contain extensive analysis.

- CONTRACTOR REPORT. Scientific and technical findings by NASA-sponsored contractors and grantees.

- CONFERENCE PUBLICATION. Collected papers from scientific and technical conferences, symposia, seminars, or other meetings sponsored or cosponsored by NASA.

- SPECIAL PUBLICATION. Scientific, technical, or historical information from NASA programs, projects, and missions, often concerned with subjects having substantial public interest.

- TECHNICAL TRANSLATION. English-language translations of foreign scientific and technical material pertinent to NASA's mission.

Specialized services also include creating custom thesauri, building customized databases, and organizing and publishing research results.

For more information about the NASA STI program, see the following:

- Access the NASA STI program home page at <http://www.sti.nasa.gov>

- E-mail your question via the Internet to <help@sti.nasa.gov>

- Fax your question to the NASA STI Help Desk at 301–621–0134

- Phone the NASA STI Help Desk at 301–621–0390

- Write to:
  NASA STI Help Desk
  NASA Center for AeroSpace Information
  7115 Standard Drive
  Hanover, MD 21076–1320

NASA/TM—2007–215074

Capillary Liquid Acquisition Device Heat Entrapment

L.G. Bolshinskiy
Jacobs Engineering MSFC Group/The University of Alabama in Huntsville, Huntsville, Alabama

L.J. Hastings
Alpha Technology, Inc., Huntsville, Alabama

G. Statham
Jacobs Engineering MSFC Group/ERC Inc., Huntsville, Alabama

J.B. Turpin
Marshall Space Flight Center, Marshall Space Flight Center, Alabama

National Aeronautics and
Space Administration

Marshall Space Flight Center • MSFC, Alabama 35812

September 2007

Acknowledgments

The authors wish to extend their appreciation for the excellent technical support by Keith Hastings, who led the test apparatus assembly and testing, and for the overall technical support provided by personnel at the Hydrogen Hazardous Test Facility, Building 4628. The authors would also like to extend their thanks for the patient support of: Joe Howell, the 'In-Space Cryogenic Propellant Depot' project lead; Sue Motil, Michael Doherty, and Terri Tramel in the 'Propulsion and Cryogenics Advanced Development' project office; and Stephen Tucker, the CFM Team Lead.

TRADEMARKS

Trade names and trademarks are used in this report for identification only. This usage does not constitute an official endorsement, either expressed or implied, by the National Aeronautics and Space Administration.

Available from:

NASA Center for AeroSpace Information
7115 Standard Drive
Hanover, MD 21076–1320
301–621–0390

This report is also available in electronic form at
<https://www2.sti.nasa.gov>

TABLE OF CONTENTS

LIST OF FIGURES

LIST OF FIGURES (Continued)

LIST OF TABLES

LIST OF ACRONYMS AND SYMBOLS

CFD	computational fluid dynamics
LAD	liquid acquisition device
LN_2	liquid nitrogen
OMS	orbital maneuvering system
Ra	Rayleigh Number
RCS	reaction control system

TECHNICAL MEMORANDUM

CAPILLARY LIQUID ACQUISITION DEVICE HEAT ENTRAPMENT

1. BACKGROUND

If cryogenic propellants are used in orbital maneuvering systems (OMSs) and reaction control systems (RCSs), surface tension liquid acquisition devices (LADs) are likely to be required to ensure the supply of vapor-free propellant in the reduced gravity environment. Despite the fact that LADs have been used extensively in space-based storable propellant systems, there have been no on-orbit applications with cryogenic propellants. Although the principles of surface tension are the same for both storable and cryogenic liquids, and the LAD components should be similar, there are additional thermal control challenges inherent in the cryogen application.

1.1 Natural Convection/Thermal Stratification

Typically the heat leak into a cryogenic container must be carefully controlled to avoid excessive boil-off and ensure adequate pressure control. Despite careful thermal engineering intended to minimize heat leaks, natural convection can occur and result in significant circulation patterns that, in turn, affect the degree of thermal stratification. Stratification, or the distribution of thermal energy within the cryogenic tank and feed system, must be considered in ensuring propellant subcooling sufficient to avoid cavitation and vapor formation during propellant outflow to the engine.

A common misconception is that natural convection is insignificant in microgravity. However, even in a microgravity environment on the order of 10^{-4}g, convective currents can be established, as illustrated in figure 1.

Convection will occur provided the Rayleigh Number (Ra) is sufficiently large. Ra is defined as follows:

$$Ra = \frac{g\alpha\Delta T d^3}{\nu\kappa} \quad , \tag{1}$$

where:

g = acceleration
α = coefficient of thermal expansion
ΔT = temperature differential
d = length scale
ν = kinematic viscosity
κ = thermal diffusivity.

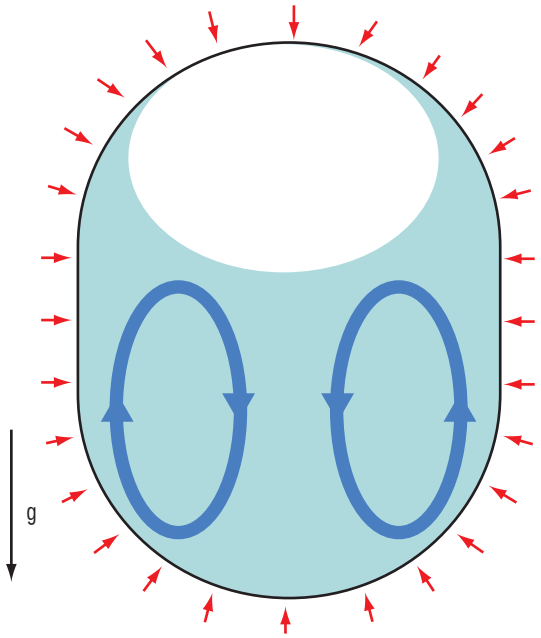

Figure 1. Natural convection circulation patterns.

As an example, during the Apollo Program, convection was observed in the hydrogen tank of an orbiting Saturn S-IVB test stage during the Saturn AS-203 Flight Experiment.[1] After the main test operations were complete, the 6.1-m (20-ft) -diameter hydrogen tank, containing some 16,000 lb of residual liquid, was isolated—i.e., the vent system was closed—to observe self-pressurization in reduced gravity. At the same time, a gaseous oxygen ullage settling system was used to provide a positive acceleration to the vehicle. This slight acceleration, which decreased from 3.7×10^{-4} g at the start of the test to 0.8×10^{-4} g at the end, was sufficient to settle the liquid hydrogen. Temperature sensors within the hydrogen tank detected a 2.8 K (5 °R) axial gradient or stratification within the liquid. This gradient was attributed to the development of a convective recirculation current in the liquid. The considerable convection within the large, high-heat-leak (31,000 W), S-IVB hydrogen tank was recently substantiated using computational fluid dynamics (CFD) modeling.[2] Further, subsequent CFD modeling has demonstrated that significant convection would also occur in a 3.3-m (10-ft) -diameter tank with a much smaller heat leak of 54 W.

1.2 Liquid Acquisition Devices

As mentioned earlier, although the principles of surface tension are the same for both storable and cryogenic liquids, and the LAD components, such as screens, sponges, vanes, etc., should be similar, there are additional challenges inherent in the cryogen application. Figure 2 shows a notional cryogenic propellant tank and associated LAD concept.

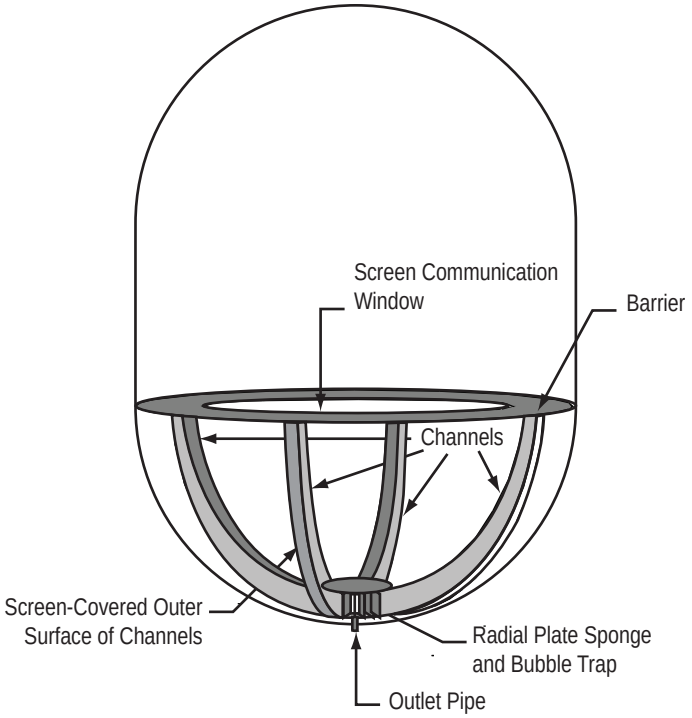

Figure 2. Representative LAD concept.

Specific details of the LAD design and operation are unnecessary beyond the following:

- A solid plate barrier with a screen communication window divides the tank into two compartments such that a significant portion of the bulk propellants is always positioned in the lower compartment. The woven mesh screen communication window permits relatively unimpeded liquid flow between the compartments, but resists gas/vapor transfer.

- The lower compartment contains screen-covered channels to acquire liquid from several different locations; i.e., independent of liquid position.

This typical LAD design is intended to support:

- OMS engine firings at the start of tank operation, with the net acceleration vector aligned along the tank main axis.

- Short-duration RCS engine firings, with acceleration vectors not necessarily aligned along the tank main axis.

1.3 Program Objectives

Precise details of LAD operation are not relevant here; however, the presence of the LAD can affect cryogenic propellant conditioning and vice versa. The presence of the solid barrier or a

compartmented tank is significant, because it can impede mixing and complicate reduced gravity pressure control. However, the issue of concern for this effort is the localized accumulation of thermal energy within the LAD flow channels. As mentioned earlier, during propellant outflow, subcooled conditions throughout the tank must be ensured to avoid undesirable cavitation and vapor formation. Since the LAD interfaces directly with the feed system, which can be a significant heat leak source, the accumulation of thermal energy within the LAD channels is of special concern (see fig. 3).

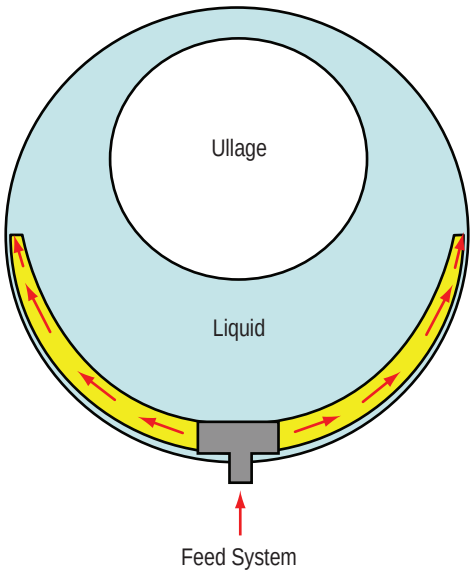

Figure 3. Thermal energy distributions within LADs.

The fundamental question addressed by this program is: "To what degree are natural convection and the resultant mixing in a cryogenic liquid constrained by the capillary screen meshes envisioned for the LADs; i.e., how does one analytically model the effect of screen meshes on natural convection?"

Whether or not the constrained convection leads to an unacceptable degree of localized stratification is not the subject of this investigation, since such a determination is dependent on specific engine operational requirements, tank/feed system thermal characteristics, the propellant, vehicle orientation, and mission profile. However, once the potential for accumulating thermal energy within LAD channels can be quantified, measures to mitigate the problem can be devised with more confidence. At present, the problem mitigation is expected to involve one or more of the following actions:

- Actively cool parts of the tank, including the LAD and/or feed line.
- Formulate appropriate interface control documentation requirements for the feed line and tank penetration interfaces.
- Establish recirculation currents within the LAD and/or feed system.

2. EXPERIMENT HARDWARE AND PROCEDURES OVERVIEW

The basic experimental approach was to heat the bottom of a cylindrical column of test fluid to establish stratification patterns measured by temperature sensors located throughout the tank. As shown in figure 4, testing was first conducted without the presence of a screen; then, the test condition was repeated with a screen placed horizontally across the test cylinder at about the halfway position of the liquid column. Finally, for reference purposes, a solid barrier was placed across the liquid column at the halfway position above the heater. The initial test series was conducted with water as the test fluid in a transparent container. The second test series was conducted with liquid nitrogen (LN_2) in a Dewar. Further details regarding the screen samples and testing with water and LN_2 are presented in sections 3 and 4 respectively.

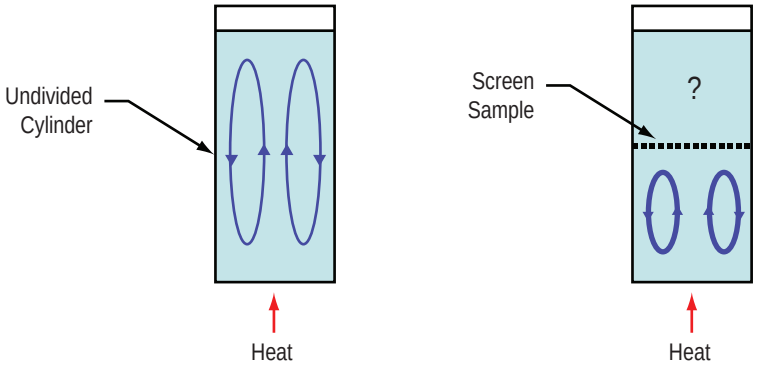

Figure 4. Heat entrapment experiment concept.

Two types of screen material were obtained for use in the tests. Both were of the stainless steel Twill Dutch Weave configuration that is typically used by surface tension LAD designers. The wire pattern used in this type of mesh is illustrated in figure 5.

The two screen meshes typically used by LAD designers, 200×1400 and 325×2300, differ in wire size and the number of warp and shute wires per unit length, as follows:

- Coarse mesh: 200 warp wires per inch, each with a diameter of 0.0028 in;
  1400 shute wires per inch, each with a diameter of 0.0016 in.

- Fine mesh: 325 warp wires per inch, each with a diameter of 0.0015 in;
  2300 shute wires per inch, each with a diameter of 0.0010 in.

Twill Dutch: Each shute wire successively passes over and under two of the warp wires. This weave type places successive shute wires very close to each other, resulting in a tightly woven filter cloth with very small tapered or wedge shaped openings.

With acknowledgments to the Newark Wire Cloth Company.

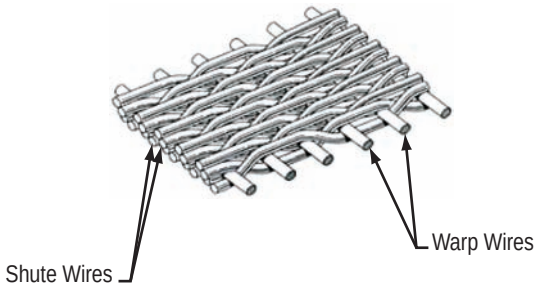

Figure 5. Dutch weave screen schematic.

3. WATER EXPERIMENT

3.1 Water Test Setup

The water test setup, shown schematically in figure 6, consisted of a double-walled transparent polycarbonate cylindrical container. The interior cylindrical container internal diameter was 19.1 cm and its height was 106 cm. The exterior cylinder was used to form a 2.54-cm annulus that could be evacuated, thereby minimizing sidewall heat leakage into the liquid. Thermal energy was injected into the water through two independent heaters located at the bottom of the tank. By monitoring current and voltage in the heater circuits, the thermal energy injected into the water could be quantified. Temperature sensors—thermocouples—were located at two positions above and below the screen sample, which was positioned 45.7 cm above the tank base. As illustrated in figure 7, five sensors were mounted on a cross-shaped support structure at each of the four measurement positions shown in figure 6.

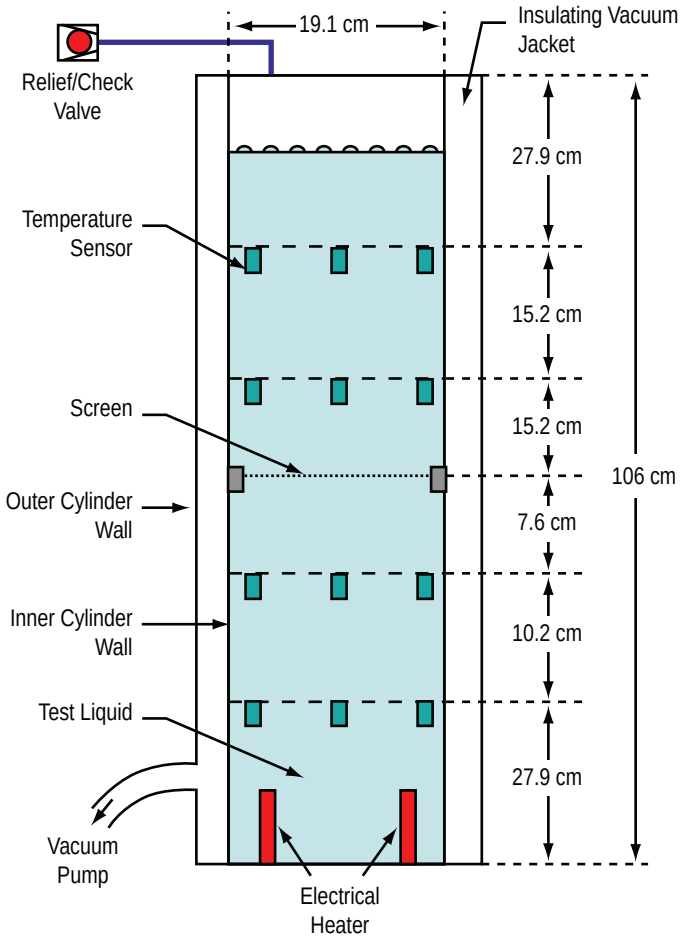

Figure 6. Heat entrapment water experiment configuration.

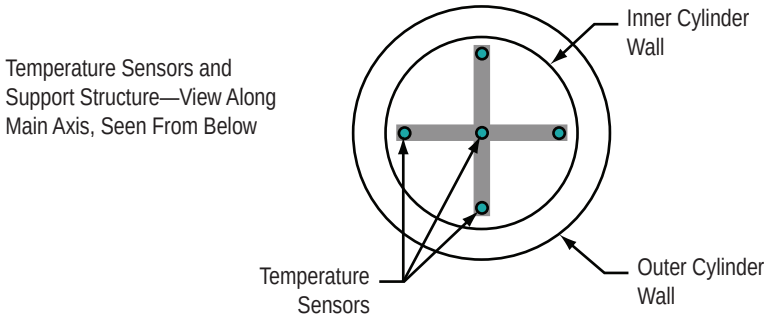

Figure 7. Radial sensor distribution at each measurement level.

With the same sensor pattern replicated at each position or level, detailed measurements of the test liquid thermal state could be obtained. Referring to figure 8, the four measurement levels are designated as follows:

- Top: 76.2 cm above the base; 30.4 cm above the screen.
- Upper-Middle: 61.0 cm above the base; 15.2 cm above the screen.
- Lower-Middle: 38.1 cm above the base; 7.6 cm below the screen.
- Bottom: 27.9 cm above the base; 27.8 cm below the screen.

At each level the sensors are designated Front, Back, Left, Right, and Center.

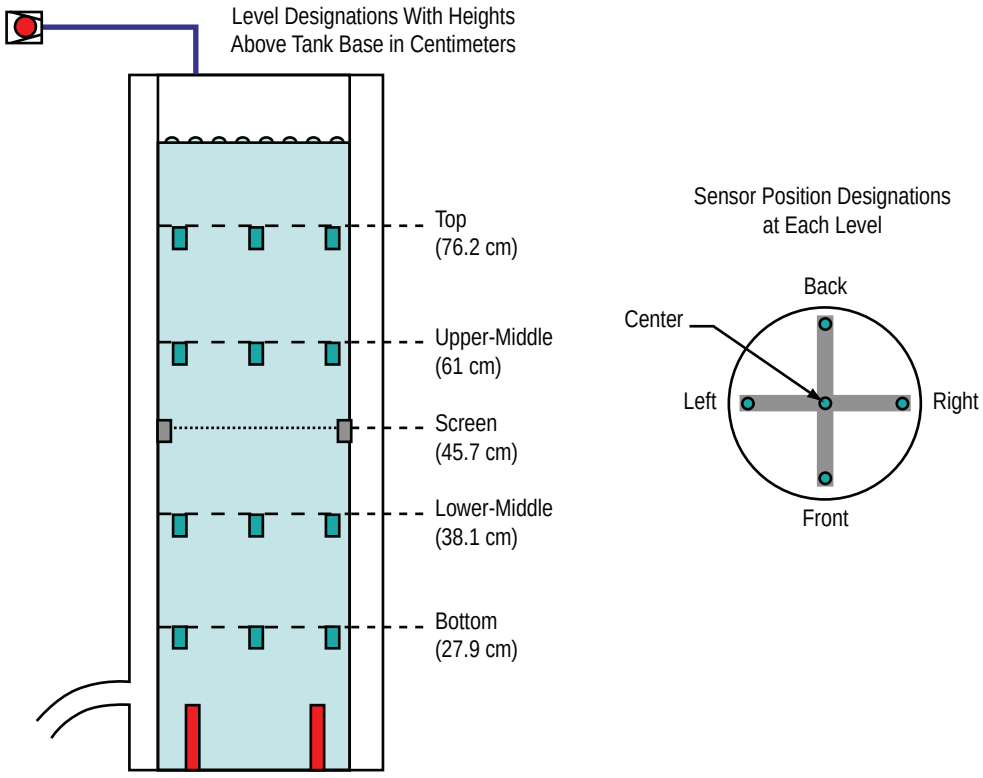

Figure 8. Instrumentation arrangement/designation diagram.

Photographs of the actual test cylinder, loaded with water, and one of the cross-shaped support structures, holding five temperature sensors, are presented in figures 9 and 10, respectively.

Figure 9. Water test setup.

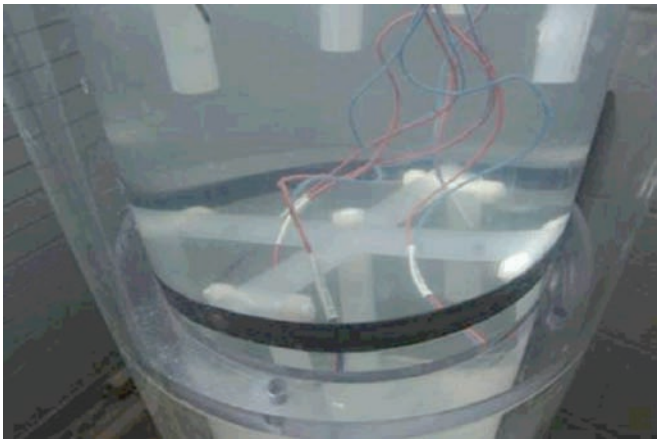

Figure 10. Temperature sensor support structure.

3.2 Water Experiment Approach

Checkout testing was conducted first to ensure that the test setup functioned satisfactorily. The baseline testing was performed after problems discovered during the checkout phase were corrected. In either case, the test matrix presented in table 1 guided the test sequence. The matrix reflects testing first without barriers at two heater power settings, 920 and 1,840 W, followed by tests with the solid aluminum foil or solid barrier. Then the coarse mesh—200×1400—and fine mesh—325×2300—screen tests were conducted.

Table 1. Water test matrix.

Test Type	Sample Type	Approximate Heater Power (W)
Low power baseline test with no barrier	None	920
High power baseline test with no barrier	None	1,840
Low power baseline test with solid barrier	Aluminum foil	920
High power baseline test with solid barrier	Aluminum foil	1,840
Low power test with coarse screen	200×1400 screen	920
High power test with coarse screen	200×1400 screen	1,840
Low power test with fine screen	325×2300 screen	920
High power test with fine screen	325×2300 screen	1,840

3.3 Water Checkout Testing

Checkout testing was conducted first without screen barriers and then with the solid barrier, as follows:

(1) The test cylinder was set up with no barrier installed, and filled with water. The bottom of the cylinder was heated so as to set up a convective current. The resulting temperatures at several levels, from bottom to top, were recorded over a period of time. The temperature profiles showed evidence of significant convective mixing: temperatures increased in both bottom and top regions of the cylinder, with the bottom regions being slightly hotter than the top.

(2) The test cylinder was next set up with the solid aluminum foil barrier installed at the midpoint, and the cylinder was filled with water. Then one heater was activated and the resulting temperatures at several levels were recorded for 20 to 30 min. Compared with the results from the tests with no samples, the temperature profiles indicated greatly reduced thermal mixing in the cylinder; i.e., the water under the plate became hot and that above the plate remained cool.

Following the solid barrier checkout testing, the coarse screen barrier, 200×1400 mesh, was tested, and a significant problem was discovered. As the test progressed, gas bubbles began to accumulate on the underside of the screen sample, as shown in the photograph (fig. 11). These bubbles, which originated in the region of the heater, grew in number until coalescence formed a large gas pocket.

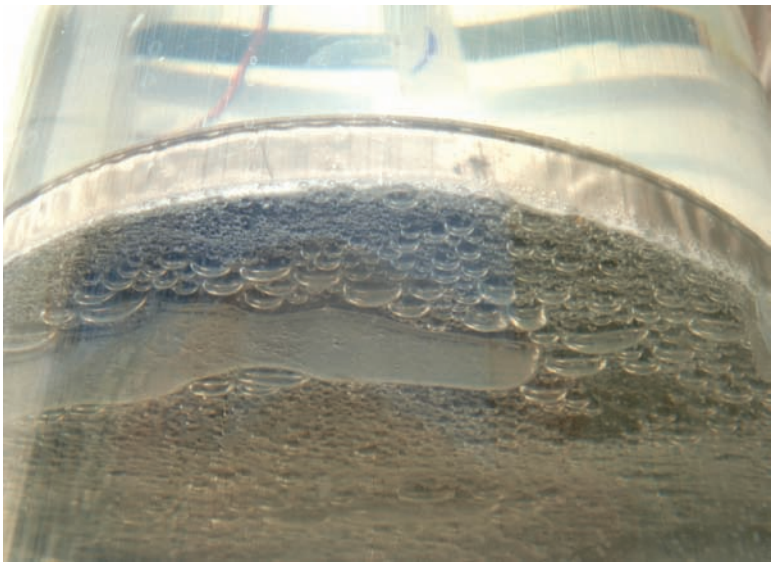

Figure 11. Gas bubble formation under screen.

Although some water vapor bubbles around the heater were expected, it was thought the bubbles would collapse as soon as they rose into the cooler liquid near the screen. However, both oxygen and nitrogen are soluble in water, and in both cases the solubility levels reduce with increasing temperature. That fact, combined with the persistence of the observed vapor accumulation, indicated that the vapor was of atmospheric origin. The gas was clearly coming out of solution in the hot region around the heater, and at least some of it was subsequently remaining out of solution in the generally elevated temperatures. Since the gas beneath the screen acted as an obstacle to convective flow, it was of significant concern.

Subsequently, two potential techniques to mitigate the effects of gas entrapment were investigated. The first involved attaching a weight to the center of the screen, pulling it down slightly. It was thought that gas would migrate to the periphery of the tank, leaving the major part of the screen unimpeded. Unfortunately, when this technique was attempted, the gas volume was large enough to block a significant portion of the screen, as illustrated in figure 12. There were also concerns that the distorted screen might have undesirable effects on flow patterns.

The second technique focused on removing the majority of the dissolved gasses from the water before testing began. It is known that gas solubility levels decrease as the liquid temperature increases. Accordingly, before the screen sample was placed in the cylinder, the water was heated continuously for a period of at least a day. This period of heating was intended to drive off a large portion of the dissolved atmospheric gases. The water was subsequently allowed to cool before the screen was inserted and testing began. Although the equilibrium solubility level increases as the liquid cools, the amount of gas returning to solution was minimized by ensuring that the liquid was not agitated. Once it had been 'de-aerated,' the water was not changed between successive tests, nor agitated unnecessarily. With these modified procedures, the vapor accumulation problem was resolved and testing was allowed to proceed.

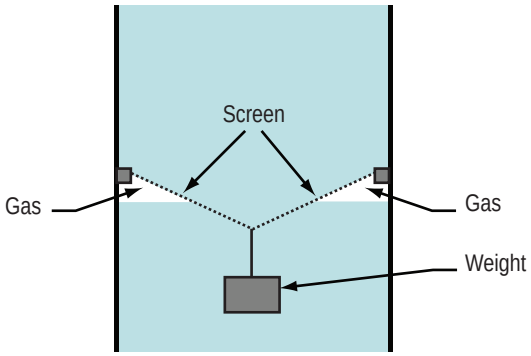

Figure 12. Gas accumulation under distorted screen.

3.4 Baseline Water Test Results

Considerable convective mixing occurred throughout the testing, making a sensor-to-sensor comparison impractical and misleading. Furthermore, due to complex mixing currents at the 'Bottom' positions, near the heaters, and the uppermost or 'Top' positions, the temperature trends at these positions were not necessarily reflective of what was occurring at or near the screen position.* However, the averaged temperatures at the positions or levels nearest the screen, i.e., the Lower-Middle and Upper-Middle positions, enabled a clear evaluation of convective flow resistance due to the barriers. Also, it is emphasized that any temperature magnitudes presented herein are considered adequate to establish relative, but not absolute, heat transfer resistance characteristics.

The test results for the Lower-Middle and Upper-Middle positions—7.6 cm below screen and 15.2 cm above the screen, respectively—are graphed in figures 13–16. Temperature vs. time histories for the two screen meshes, the solid barrier, and no barriers for test durations ranging from 40 to 50 min are presented for the low heater setting, 920 W, in figures 13 and 14 and for the high heater setting, 1,840 W, in figures 15 and 16. During tests with a barrier, temperatures below the barrier position consistently increased more rapidly than without the barriers, indicating the accumulation of thermal energy or heat entrapment. For example, at the end of the 920-W test period (≈50 min), the Lower-Middle temperatures (below the barrier position) were 5 to 10 °C higher with the barriers, as shown in figure 13. Similarly, at the 1,840-W setting, temperatures were 13 to 16 °C higher due to the presence of the barriers, as shown in figure 15. Conversely, temperatures at the Upper-Middle—above the barrier—position were lower with the barriers. With the barriers installed, the Upper-Middle temperatures at the end of the test with the 920-W setting were 10 to 11 °C lower, as shown in figure 14, and, at the 1,840-W setting, were 16 to 19 °C lower, as shown in figure 16.

Therefore, it can be concluded that all the water tests performed with samples installed, whether coarse screen, fine screen, or solid barrier, indicated greatly reduced thermal mixing. Also, although the solid plate represents a complete barrier against convective flow, the plate actually showed a greater amount of heat transfer than either of the two mesh samples. The reason for this is that the aluminum barrier has a higher thermal conductivity than that of the stainless steel screen mesh. Additionally, contrary to what one might expect, slightly more heat transfer occurred across the fine mesh screen than

* Data for the Top and Bottom positions is presented in Appendix A.

with the coarse mesh. Apparently, neither mesh allowed the passage of convective currents; however, the fine mesh—being considerably thinner—allowed a greater degree of thermal conduction from the lower to the upper compartment. Nevertheless, both the screen samples showed greater heat entrapment than the solid barrier. This appears to be conclusive proof that, with water as the test fluid, the screens effectively prevented the passage of natural convection.

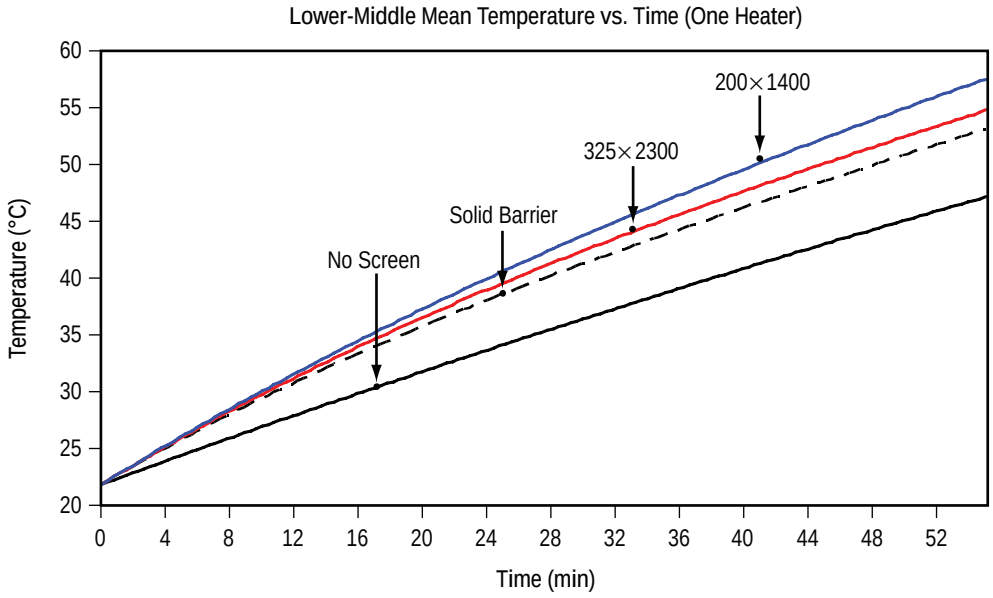

Figure 13. Average Lower-Middle position temperature vs. time at low power.

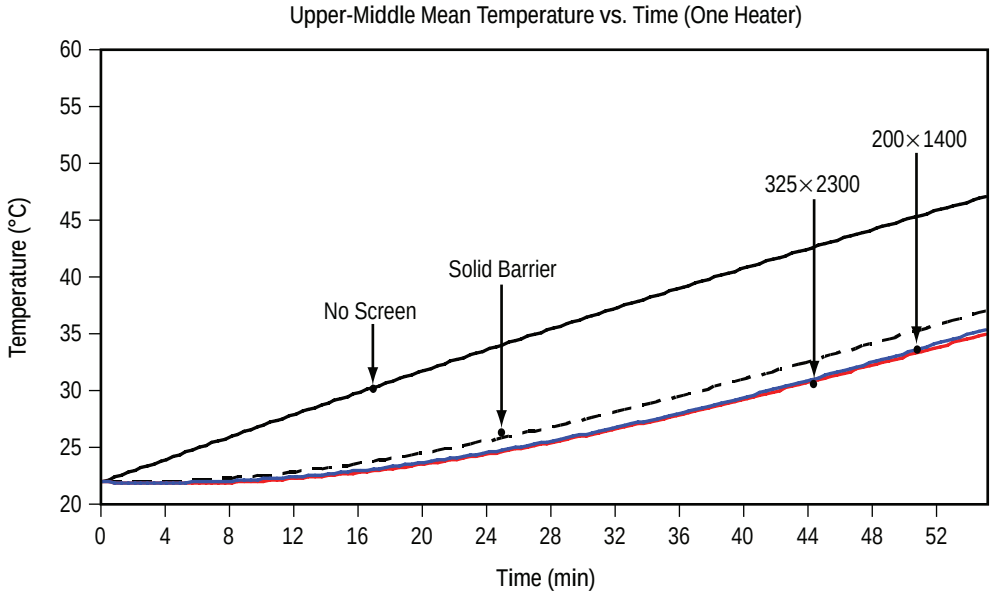

Figure 14. Average Upper-Middle position temperature vs. time at low power.

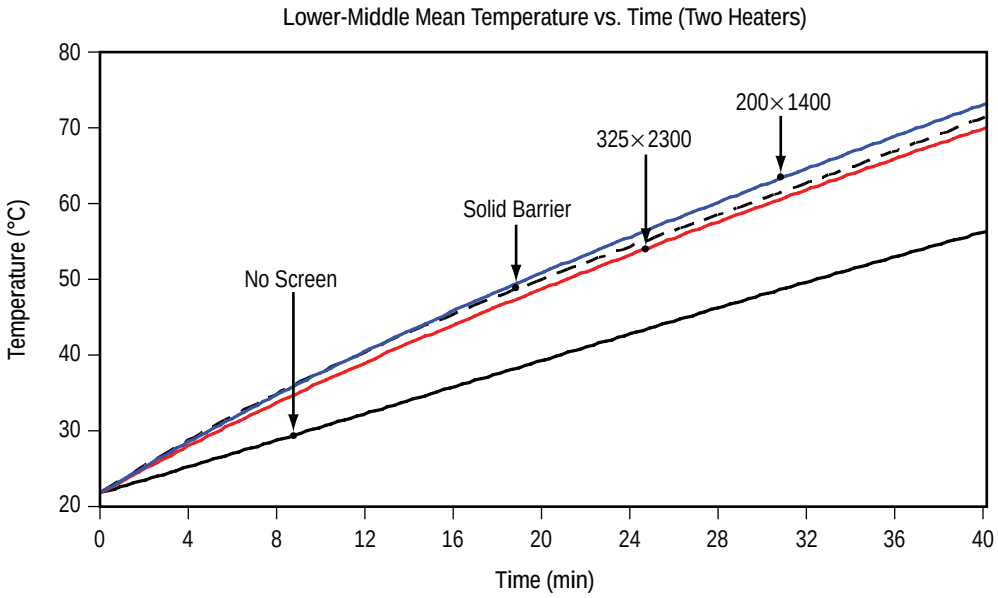

Figure 15. Average Lower-Middle position temperature vs. time at high power.

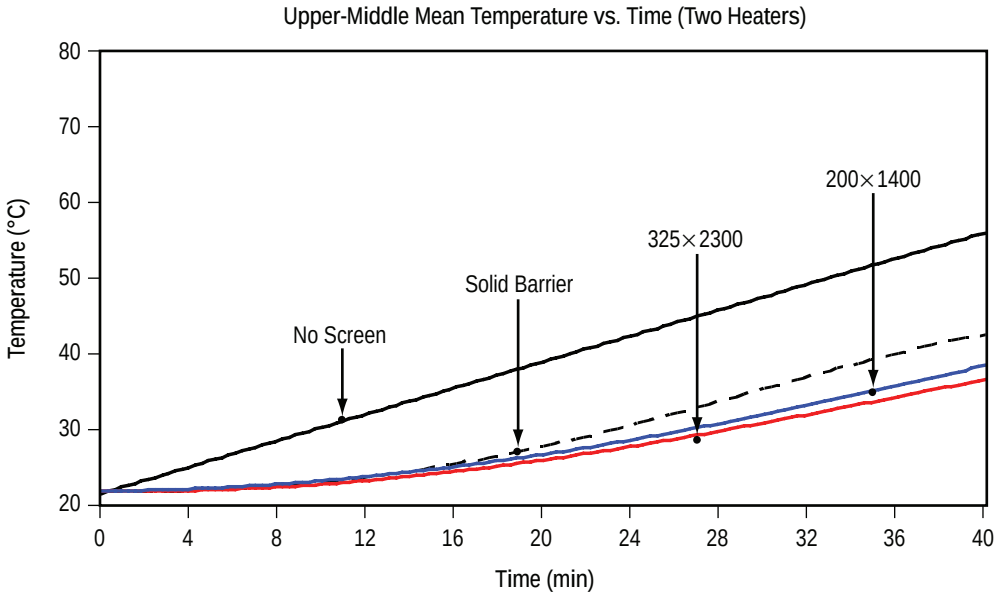

Figure 16. Average Upper-Middle position temperature vs. time at high power.

Therefore, it is concluded that, with water as the test fluid, the 200×1400 and 325×2300 capillary screen meshes typically anticipated for LAD applications both represented barriers impervious to natural convection currents at two heater power levels, 920 W and 1,840 W. This conclusion, however, needed to be verified with a cryogenic liquid such as LN_2, as described in section 4.

4. LIQUID NITROGEN EXPERIMENT

4.1 Liquid Nitrogen Experiment Background and Checkout Testing

Subsequent to the water experiment, preliminary stress analyses indicated that the transparent polycarbonate container used in the water testing would be safe for anticipated test conditions with LN_2. Therefore, the container, which would allow visual observation, was prepared for testing with LN_2. However, based on the final stress analyses, the container eventually was disapproved for safety reasons and the LN_2 testing reverted to the use of a stainless steel Dewar. The Dewar interior geometry comprises a diameter of 30.3 cm, a height of 77.5 cm, and a volume of 56 L. Initial testing indicated that the temperature distributions were significantly affected by the Dewar sidewall and top/bottom heat leak. The Dewar heat leak, combined with the relatively large diameter and volume, obscured the stratification created by the heater. Therefore, an alternate approach was adopted wherein a polycarbonate cylinder was installed inside the Dewar to shield the stratification created by the heater from the sidewall heating effects. Also, the checkout testing indicated that the heater-induced stratification was clearest at the maximum heater setting of ≈104 W.

4.2 Liquid Nitrogen Test Setup

The Dewar exterior is pictured in figure 17, and a schematic of the final test setup with the internal cylinder installed is presented in figure 18. The inner polycarbonate cylinder, which was the same inner cylinder used in the water tests, contained the screen sample, temperature sensors, and heater. The experiment was conducted within this restricted volume, wherein the heater was sufficient to establish an adequate level of convection and stratification. However, the entire vessel was filled with LN_2 for each test.

Therefore, the sensors' spacing relative to the barrier, tank bottom, and each other was identical to the temperature sensing positions used in the water tests. Five silicon diode temperature sensors, instead of thermocouples, were mounted on the cross-shaped support structure at each level, as illustrated in figure 19 and pictured in figures 20–23. As in the water tests shown in figure 8, the four measurement levels are referred to as Bottom, Lower Middle, Upper Middle, and Top. Also, at each level, the sensors are designated, relative to the front of the cylinder, as Center, Front, Back, Left, and Right.

Figure 17. LN_2 test setup photograph.

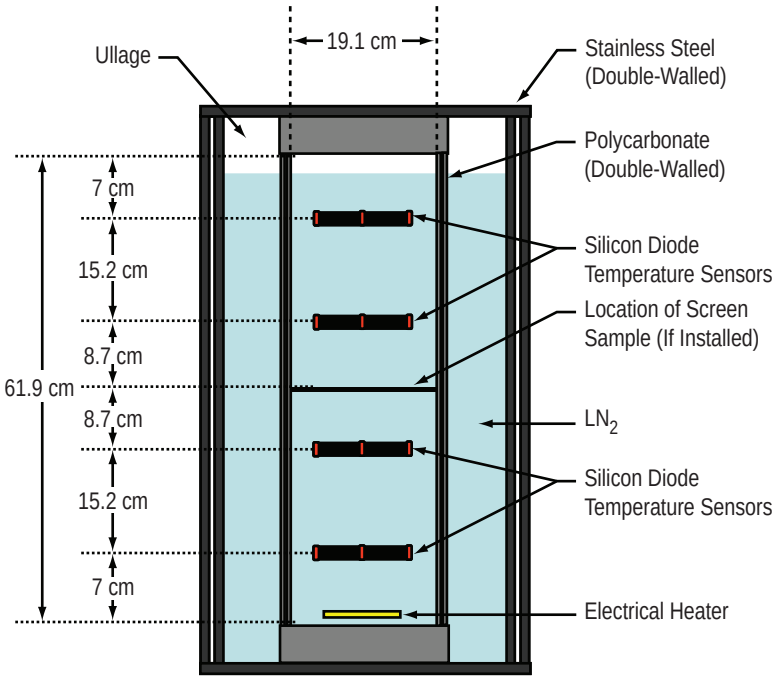

Figure 18. Heat entrapment LN_2 experiment configuration schematic.

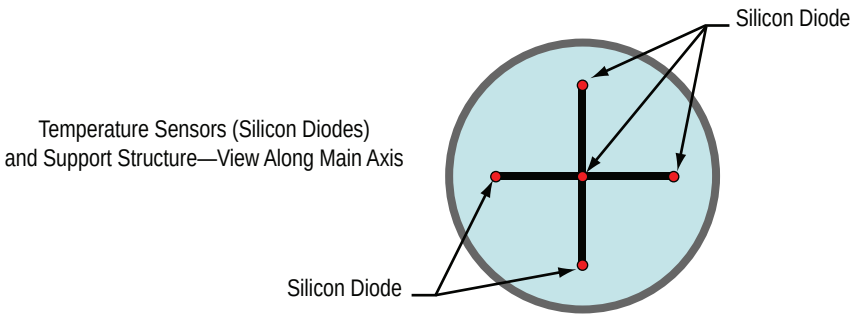

Figure 19. Radial sensor distribution at each measurement level.

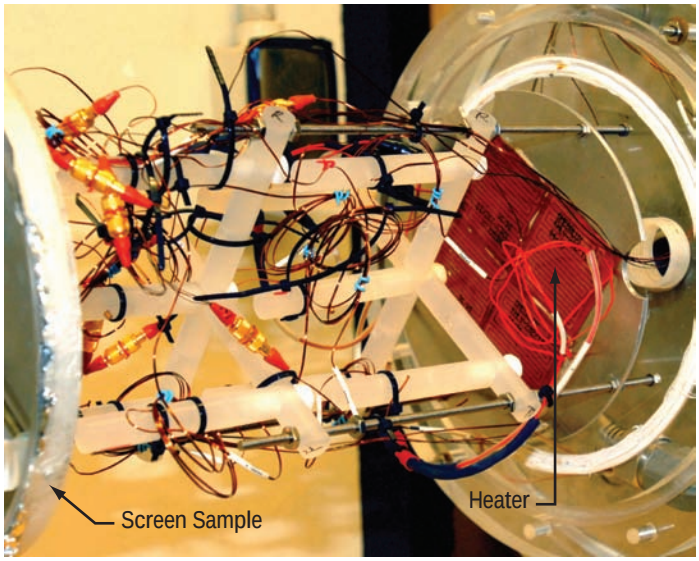

Figure 20. Temperature sensor support structure, bottom part.

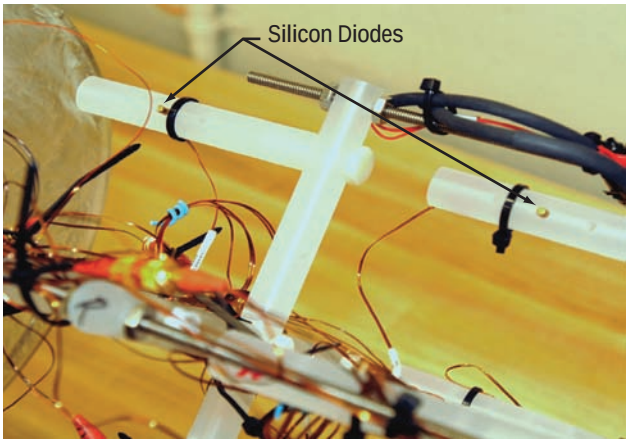

Figure 21. Silicon diodes installation.

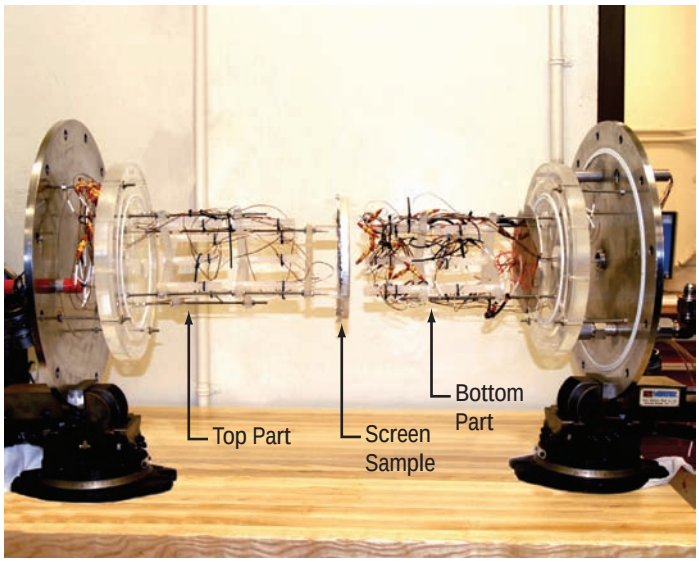

Figure 22. Temperature measurement system.

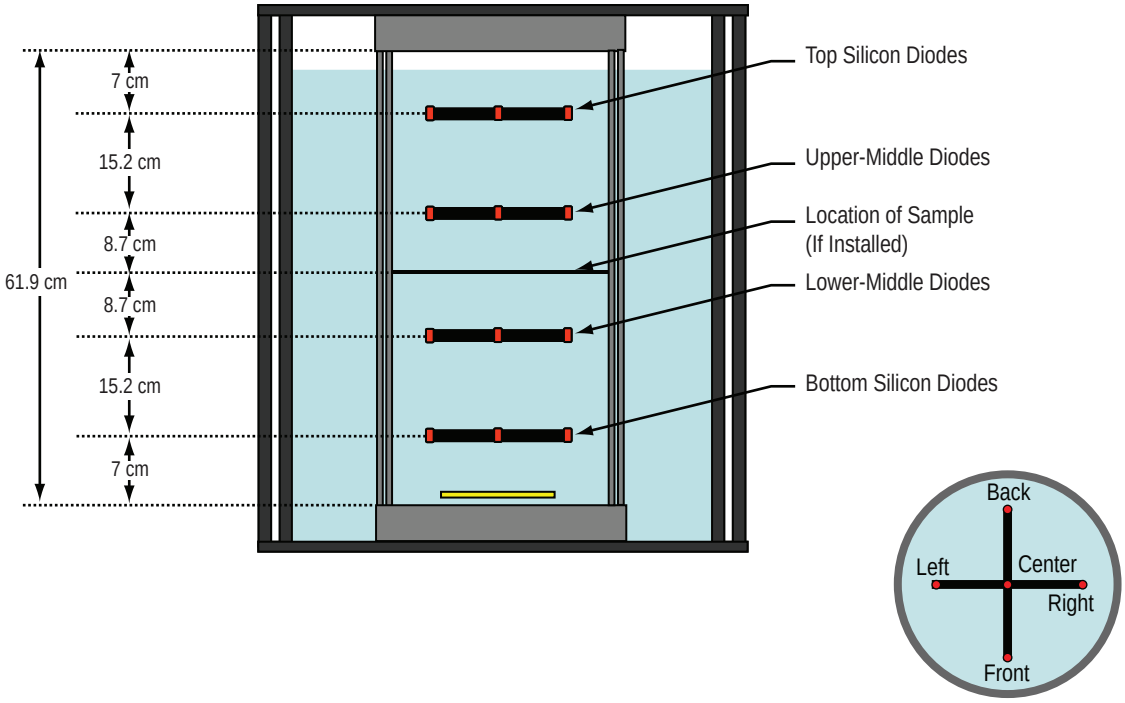

Figure 23. Instrumentation arrangement/designation diagram.

4.3 Liquid Nitrogen Test Procedure

The test matrix used to guide the testing is presented in table 2. The basic experimental approach was to achieve stable conditions within the Dewar, and then activate the heater at the bottom of the cylindrical column of test fluid to establish stratification patterns that were measured by temperature sensors located within the interior cylinder. Typically, the test duration was about 10 min, which was determined primarily by the Dewar pressure control requirements. Testing was first conducted to establish baseline stratification conditions without the presence of a screen and with and without heater activation. With this baseline condition, the cylinder was cleared of any significant obstructions—only the temperature instrumentation arrangement was present—so that unimpeded convection could occur. Then, the test condition was repeated with a screen placed horizontally across the test cylinder at about the halfway position of the liquid column, first with the 200×1400 screen mesh, and then with the 325×2300 screen mesh (see fig. 18). Finally, for reference purposes, a solid barrier of aluminum foil supported by the 325×2300 mesh screen was placed across the liquid column. In the process of testing, it was observed that care had to be taken to establish consistent initial conditions, or the temperature magnitudes for the various test conditions could not be compared.

Table 2. LN_2 test matrix.

Test Type	Sample Type	Approximate Heater Power (W)
No power baseline test with no sample	None	0
Baseline test with no sample	None	103
Test with coarse screen	200×1400 screen	103
Test with fine screen	325×2300 screen	104
Baseline test with solid barrier	Aluminum foil, supported by 325×2300 screen	104

4.4 Liquid Nitrogen Test Results

Considerable convective mixing occurred in the LN_2 tests, making individual sensor-to-sensor comparisons impractical and misleading. Furthermore, stratification created by the heater was somewhat obscured by the heat leak from the Dewar bottom and top. Because of the small temperature differences and very complex mixing currents, data at the Lower Bottom and Upper Top positions** could not be used to evaluate trends at or near the barrier position. However, as in the water tests, the averaged temperatures at the positions or levels nearest the screen—the Lower-Middle and Upper-Middle positions–enabled an evaluation of convective flow resistance trends due to the barriers. Again, it is emphasized that any temperature magnitudes presented herein are considered adequate to establish relative, but not absolute, convective flow resistance characteristics.

The test results for the Lower-Middle and Upper-Middle positions—8.7 cm below and above the screen—are graphed in figures 24–27. Temperature vs. time histories for both screen meshes, the solid barrier, and no barriers are presented for a 10-min test period in figures 24 and 25, and with an expanded scale in figures 26 and 27. The Dewar heat leak effects on the liquid temperature rise rate are clearly illustrated with the ‘no barrier, no heater’ condition; i.e., increased about 0.39 K/min. Therefore,

** Data for the Lower Bottom and Upper Top positions is presented in Appendix B.

it is evident that the temperature differences (stratification) produced by the heater were reduced by the heat leak from the Dewar bottom and top. However, even though the temperature differences are small, the trends with the barriers installed were like those observed in the earlier water tests. Referring to the expanded scale in figures 26 and 27, the temperatures below the barrier position were consistently higher with the barriers installed, indicating heat entrapment. Conversely, temperatures above the barrier position were consistently lower with the barriers installed, indicating reduced stratification.

The solid barrier case represented the greatest thermal resistance condition. Although the solid barrier condition represented total resistance against convective flow, the barrier-to-barrier temperature differences were small enough, ≈0.3 K, to have been caused by the thermal conductivity of the solid barrier—aluminum foil plus screen—compared with that with the 'screen only' conditions. Furthermore, the earlier water testing indicated that the solid barrier used in those tests—aluminum foil only—was actually less of a barrier than the screens, an effect that was also attributed to barrier thermal conductivity differences. Therefore, upon consideration of both the water and LN_2 data, one can conclude that heat transfer across the screen meshes evaluated is dependent upon thermal conduction and that the passage of natural convection through the screens was effectively blocked. In conclusion, it is recommended that future LAD heat entrapment thermal analyses consider only thermal conduction across capillary screen barriers with either 200×1400 or 325×2300 meshes.

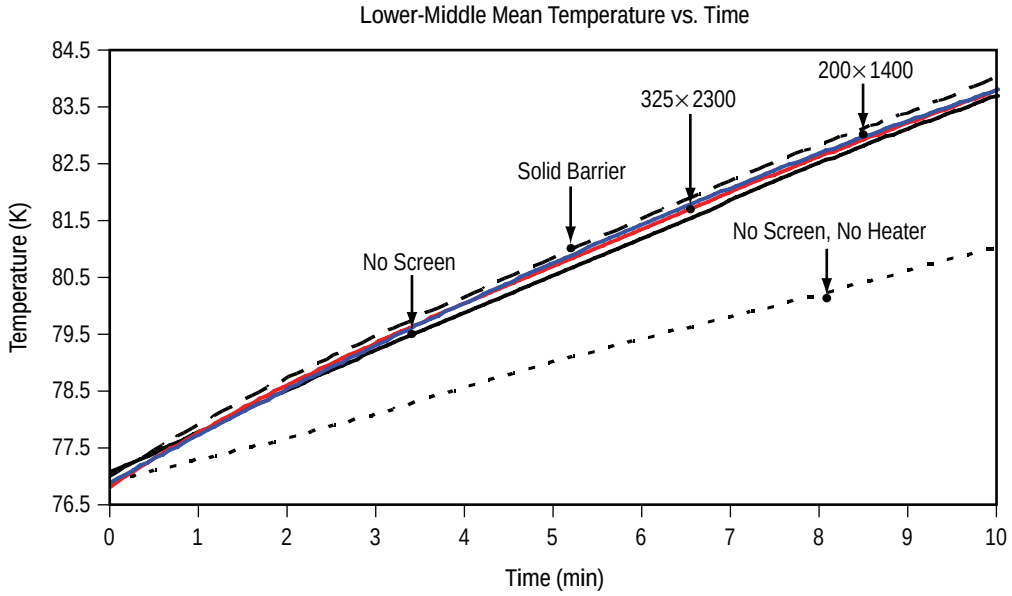

Figure 24. Average Lower-Middle position temperature vs. time.

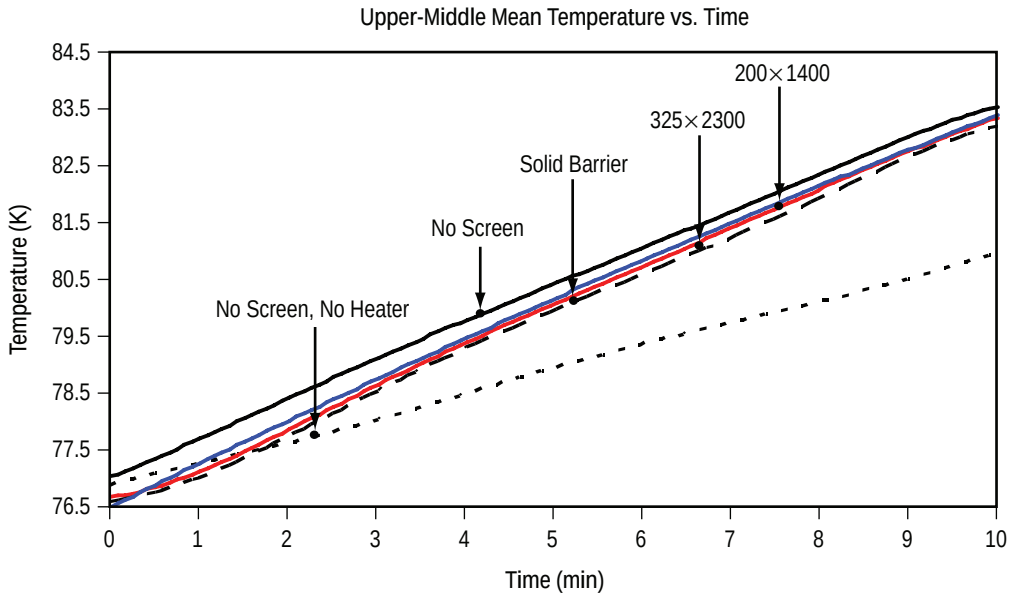

Figure 25. Average Upper-Middle position temperature vs. time.

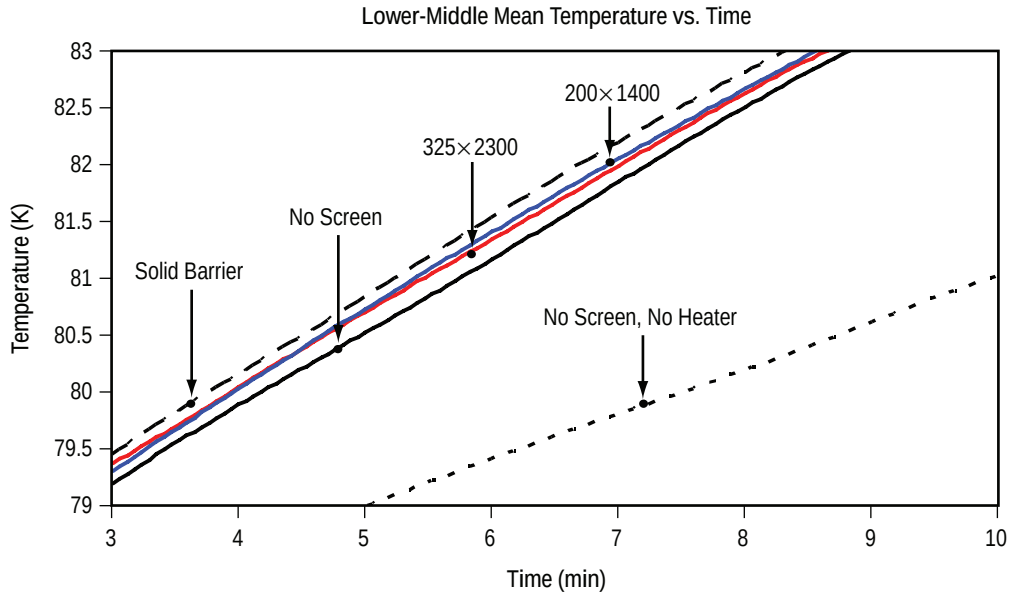

Figure 26. Average Lower-Middle position temperature vs. time, expanded scale.

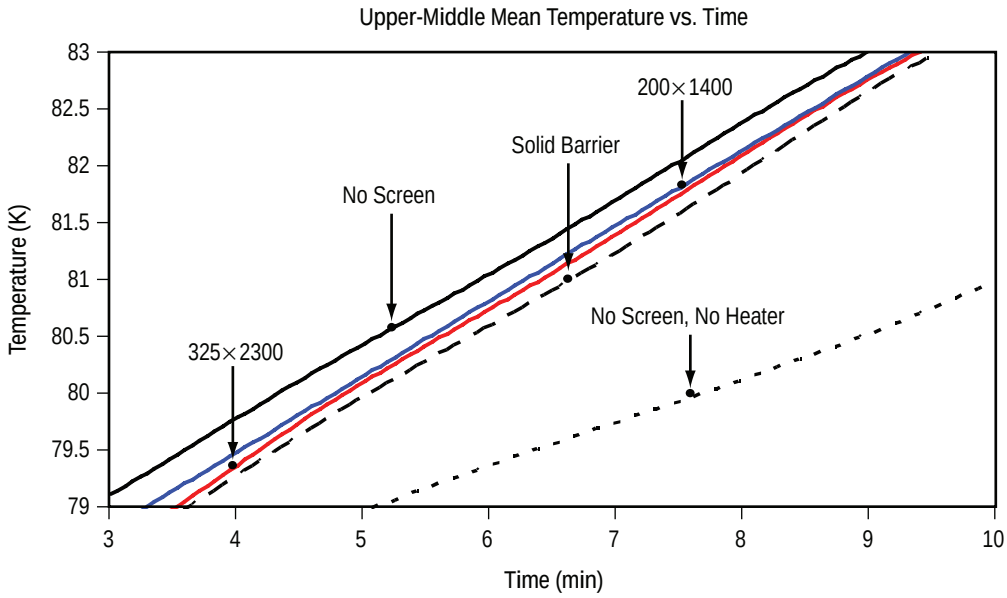

Figure 27. Average Upper-Middle position temperature vs. time, expanded scale.

5. SUMMARY AND RECOMMENDATIONS

Despite the fact that capillary LADs have been used extensively in space-based storable propellant systems, there has been no on-orbit application with cryogenic propellants. Although the principles of surface tension are the same for both storable and cryogenic liquids, there are additional thermal control challenges inherent in the cryogen application. The issue of concern for this effort is the localized accumulation of thermal energy within the LAD flow channels. Because the LAD interfaces directly with the feed system, which can be a significant heat leak source, the accumulation of thermal energy within the LAD channels is of special concern. This accumulation can lead to the loss of subcooled propellant conditions and result in feed system cavitation during propellant outflow. Therefore, the fundamental question addressed by this program was: "To what degree are natural convection and the resultant mixing in a cryogenic liquid constrained by the capillary screen meshes envisioned for the LADs; i.e., how does one analytically model the effect of screen meshes on natural convection?"

Testing was first conducted with water as the test fluid, followed by LN_2 tests. In either case, the basic experimental approach was to heat the bottom of a cylindrical column of test fluid 19.1 cm diameter by 106 cm high to establish stratification patterns measured by temperature sensors located above and below a horizontal screen barrier position. Testing was conducted without barriers, with screens, and with a solid barrier. The two screen meshes tested were those typically used by LAD designers, 200×1400 and 325×2300, both with Twill Dutch Weave.

During the water checkout tests, air came out of solution and accumulated under the barriers, thereby affecting the test results. Subsequently test operators 'de-aerated' the water by heating it for extended periods of time and avoiding agitating it prior to testing. Test results indicated that with a barrier, temperatures below the barrier position consistently increased more rapidly than without the barriers, indicating the accumulation of thermal energy or heat entrapment. Contrary to what one might expect, slightly more heat transfer occurred across the fine mesh screen than across the coarse mesh. Neither mesh allowed the passage of convective currents; however, the fine mesh—being considerably thinner—allowed a greater degree of thermal conduction from the lower to the upper compartment. Also, although the solid plate represents the most complete barrier against convective flow, it actually showed a greater amount of heat transfer than either of the two mesh samples. Apparently this is due to the higher thermal conductivity of the aluminum barrier as compared with the stainless steel screen mesh. Therefore, with water as the test fluid, the 200×1400 and 325×2300 capillary screen meshes both represented barriers impervious to natural convection currents at two heater power levels, 920 W and 1,840 W.

LN_2 testing was conducted within a 56-L stainless steel Dewar. An inner polycarbonate cylinder, which was the same as that used in the water tests, was installed inside the Dewar to shield the stratification created by the heater from the sidewall heating effects. It is within this restricted volume that the experiment was conducted. However, stratification created by the 104-W heater was still somewhat obscured by the heat leaks from the Dewar's bottom and top.

The Dewar heat leak effects on the liquid temperature rise rate were clearly illustrated with the ‘no barrier, no heater’ condition; i.e., the temperature increased about 0.39 K/min. Therefore, it is evident that the temperature differences, or stratification, produced by the heater were reduced by the heat leak from the Dewar’s bottom and top. However, even though the temperature differences were small, the trends with the barriers installed were like those observed in the earlier water tests. The temperatures below the barrier position were consistently higher with the barriers installed, indicating heat entrapment. Conversely, temperatures above the barrier position were consistently lower with the barriers installed, indicating reduced stratification. Upon consideration of both the water and LN_2 data, one can conclude that heat transfer across the screen meshes evaluated was dependent upon barrier thermal conductivity and that the passage of natural convection through the screens was effectively blocked. In conclusion, future LAD heat entrapment thermal analyses should consider only thermal conduction across capillary screen barriers with either 200×1400 or 325×2300 meshes.

Whether or not the constrained convection leads to an unacceptable degree of localized stratification was not the subject of this investigation, because such a determination is dependent on specific engine operational requirements, tank/feed system thermal characteristics, the propellant, vehicle orientation, and mission profile. However, once the potential for accumulating thermal energy within LAD channels is quantified, measures to mitigate the problem can be devised with more confidence. At present the problem mitigation is expected to involve one or more of the following actions:

- Actively cool parts of the tank including the LAD and/or feed line.
- Formulate appropriate interface control documentation requirements for the feed line and tank penetration interfaces.
- Establish recirculation currents within the LAD and/or feed system.

APPENDIX A—WATER HEAT ENTRAPMENT TEST DATA FOR THE BOTTOM AND TOP MEASUREMENT POSITIONS

The averaged water temperatures at measurement positions furthermost from the barrier position (Bottom and Top) are graphed in figures 28–33. Measured temperature vs. time histories are presented for the low heater setting (920 W) in figures 28 and 29 and for the high heater setting (1,840 W) in figures 30 and 31. The trends were similar to those noted at measurement positions near the barriers, discussed in section 3.4, Baseline Water Test Results. Temperatures measured below the barriers increased more rapidly than temperatures measured without the barriers, indicating the accumulation of thermal energy or heat entrapment. Conversely, temperatures measured at the Top position were lower with the barriers present. Also, due to a higher thermal conductivity, the solid barrier showed a greater amount of heat transfer than either of the two screen meshes. Compared with the coarse mesh, the fine mesh allowed a greater degree of thermal conduction from the lower to the upper compartment. There was no passage of natural convection through any of the three barriers.

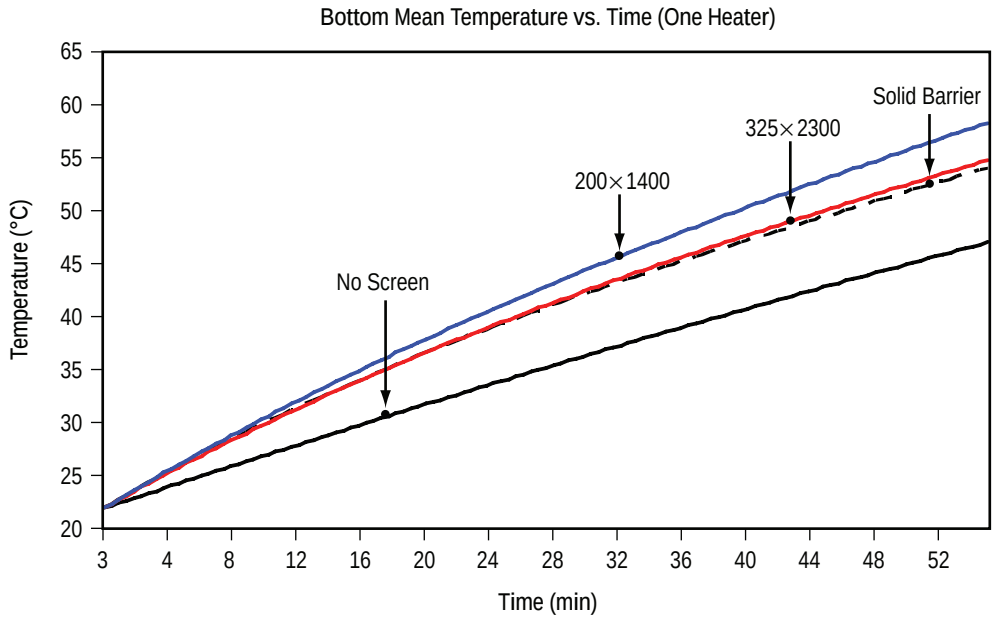

Figure 28. Average Bottom water temperature vs. time, low heater power.

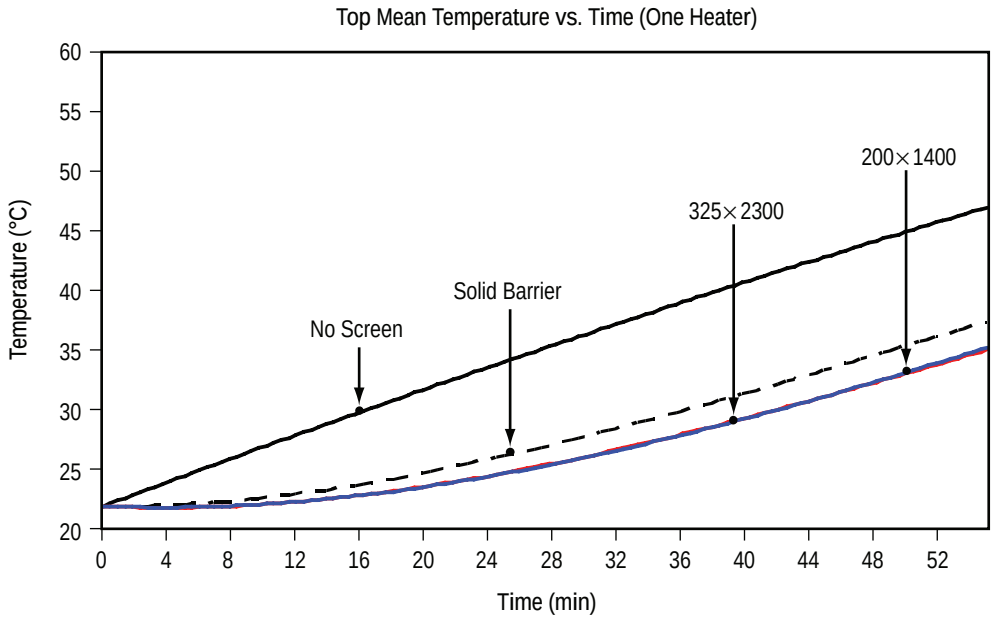

Figure 29. Average Top water temperature vs. time, low heater power.

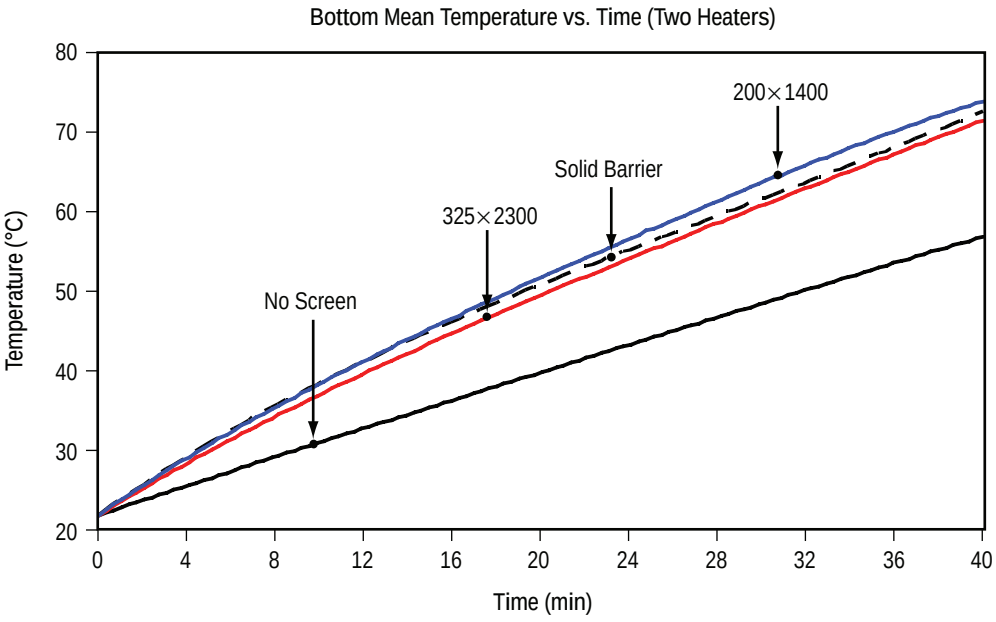

Figure 30. Average Bottom water temperature vs. time, high heater power.

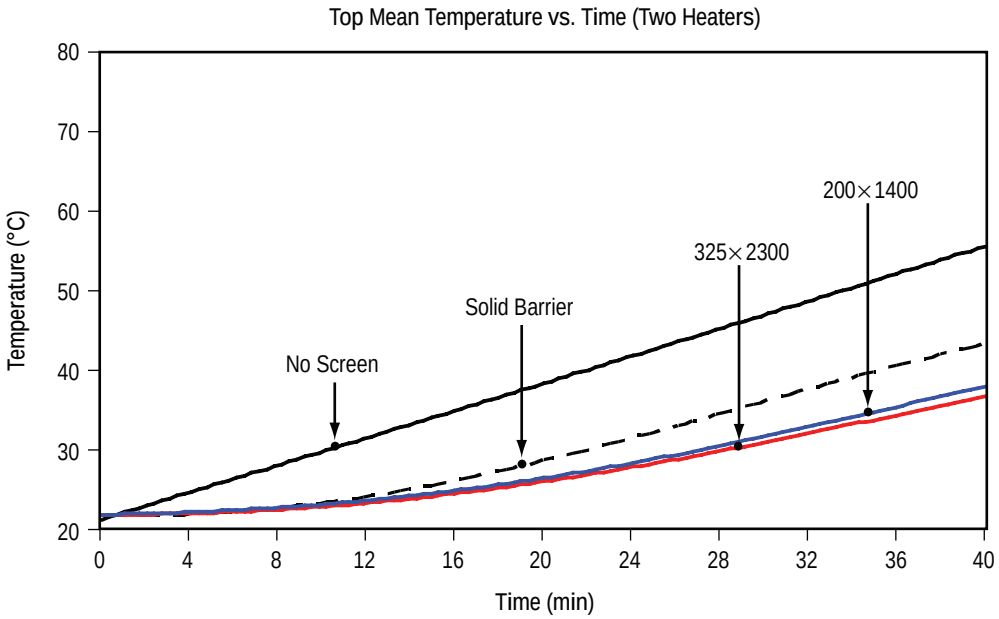

Figure 31. Average Top water temperature vs. time, high heater power.

APPENDIX B—LIQUID NITROGEN HEAT ENTRAPMENT TEST DATA FOR THE BOTTOM AND TOP MEASUREMENT POSITIONS

Measured LN_2 temperature vs. time histories for the Lower-Bottom positions, near the heater, and the Upper-Top positions are graphed in figures 32 and 33 and figures 34 and 35, respectively. However, stratification induced by the heat leak from the Dewar bottom, top, and sidewalls obscured the heater-induced stratification at these two measurement positions. The measured temperatures with the heater activated were virtually the same with and without the barriers at the Bottom position near the heater. Therefore, no trends caused by the presence of the barriers could be distinguished at this measurement position. Temperatures at the Top position were virtually the same with all the barriers, but were slightly above temperatures measured without a barrier.

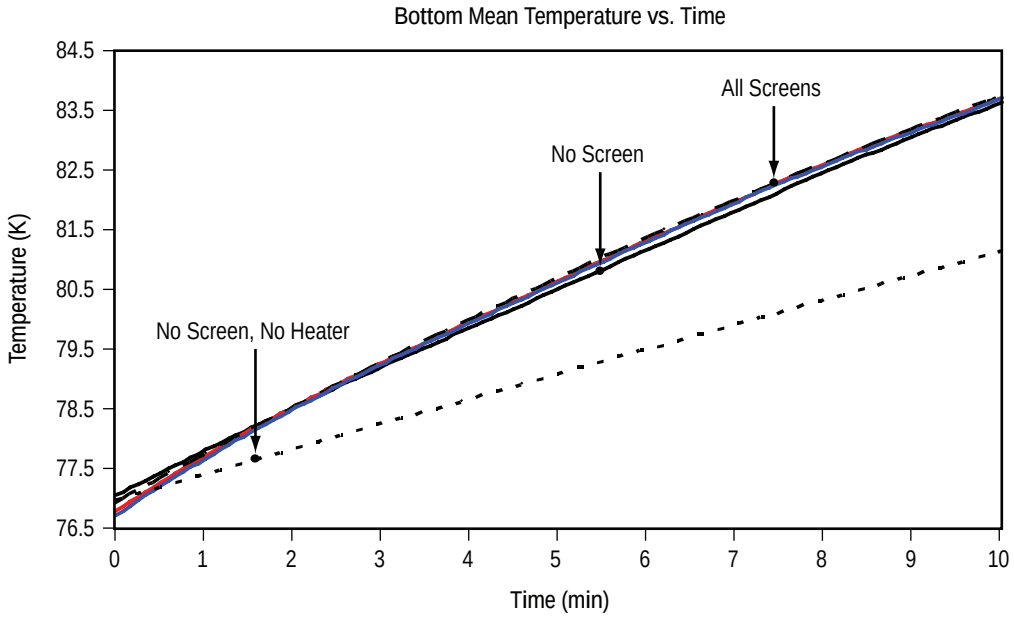

Figure 32. Average Bottom LN_2 temperature vs. time.

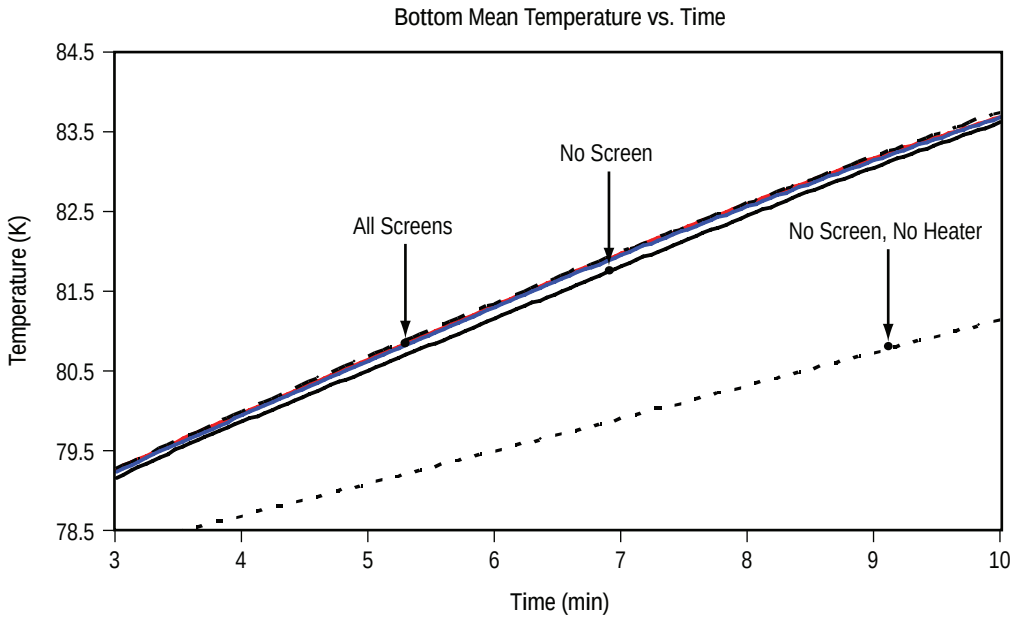

Figure 33. Average Bottom LN_2 temperature vs. time, expanded scale.

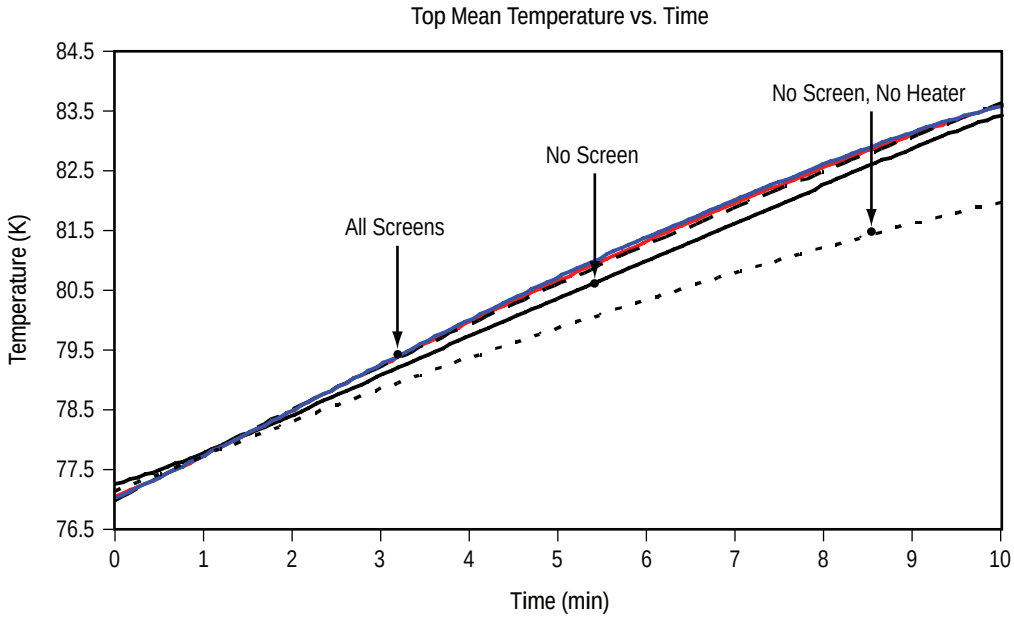

Figure 34. Average Top LN_2 temperature vs. time.

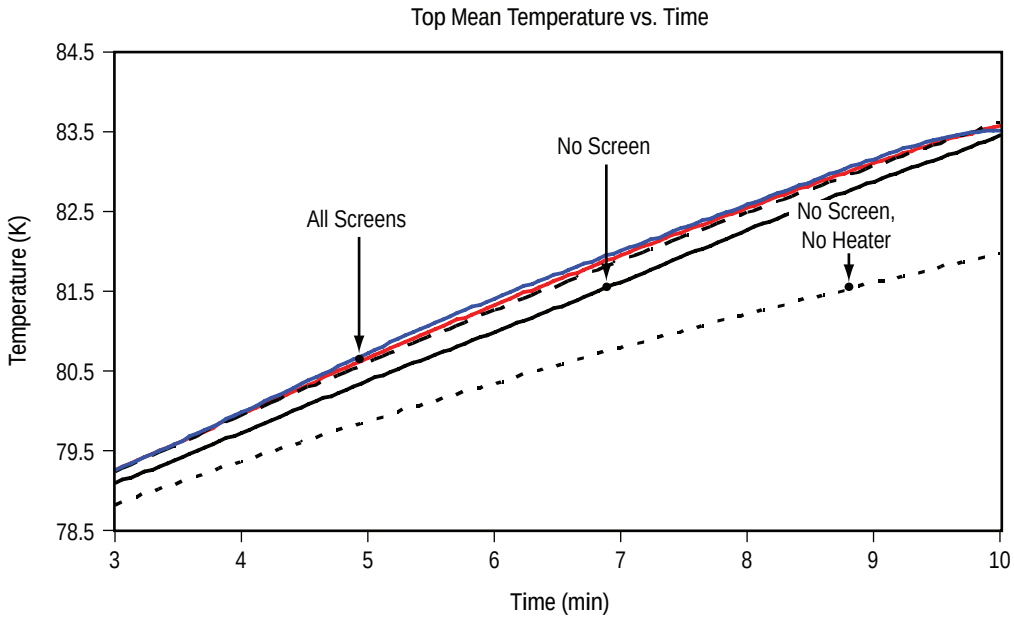

Figure 35. Average Top LN_2 temperature vs. time, expanded scale.

REFERENCES

1. "Evaluation of AS-203 Low Gravity Orbital Experiment," Chrysler Corporation, Space Division Technical Report HSM-R421-67, Contract NAS8-4016, January 1967.

2. Grayson, G.; et al.: "Cryogenic Tank Modeling for the Saturn AS-203 Experiment," AIAA paper 2006-5258, July 2006.

REPORT DOCUMENTATION PAGE

Form Approved
OMB No. 0704-0188

Public reporting burden for this collection of information is estimated to average 1 hour per response, including the time for reviewing instructions, searching existing data sources, gathering and maintaining the data needed, and completing and reviewing the collection of information. Send comments regarding this burden estimate or any other aspect of this collection of information, including suggestions for reducing this burden, to Washington Headquarters Services, Directorate for Information Operation and Reports, 1215 Jefferson Davis Highway, Suite 1204, Arlington, VA 22202-4302, and to the Office of Management and Budget, Paperwork Reduction Project (0704-0188), Washington, DC 20503

1. AGENCY USE ONLY *(Leave Blank)*	2. REPORT DATE	3. REPORT TYPE AND DATES COVERED
	September 2007	Technical Memorandum

4. TITLE AND SUBTITLE

Capillary Liquid Acquisition Device Heat Entrapment

5. FUNDING NUMBERS

6. AUTHORS

L.G. Bolshinskiy,* L.J. Hastings,** G. Statham,*** and J.B. Turpin

7. PERFORMING ORGANIZATION NAME(S) AND ADDRESS(ES)

George C. Marshall Space Flight Center
Marshall Space Flight Center, AL 35812

8. PERFORMING ORGANIZATION REPORT NUMBER

M–1200

9. SPONSORING/MONITORING AGENCY NAME(S) AND ADDRESS(ES)

National Aeronautics and Space Administration
Washington, DC 20546–0001

10. SPONSORING/MONITORING AGENCY REPORT NUMBER

NASA/TM—2007–215074

11. SUPPLEMENTARY NOTES

Prepared by the Propulsion Systems Department, Engineering Directorate
*Jacobs Engineering MSFC Group/The University of Alabama in Huntsville, Huntsville, Alabama **Alpha Technology, Inc., Huntsville, Alabama ***Jacobs Engineering MSFC Group/ERC. Inc., Huntsville, Alabama

12a. DISTRIBUTION/AVAILABILITY STATEMENT

Unclassified-Unlimited
Subject Category 16
Availability: NASA CASI 301–621–0390

12b. DISTRIBUTION CODE

13. ABSTRACT *(Maximum 200 words)*

Cryogenic liquid acquisition devices (LADs) for space-based propulsion interface directly with the feed system, which can be a significant heat leak source. Further, the accumulation of thermal energy within LAD channels can lead to the loss of subcooled propellant conditions and result in feed system cavitation during propellant outflow. Therefore, the fundamental question addressed by this program was: "To what degree is natural convection in a cryogenic liquid constrained by the capillary screen meshes envisioned for LADs?" Testing was first conducted with water as the test fluid, followed by LN_2 tests. In either case, the basic experimental approach was to heat the bottom of a cylindrical column of test fluid to establish stratification patterns measured by temperature sensors located above and below a horizontal screen barrier position. Experimentation was performed without barriers, with screens, and with a solid barrier. The two screen meshes tested were those typically used by LAD designers, 200 × 1400 and 325 × 2300, both with Twill Dutch Weave. Upon consideration of both the water and LN_2 data, it was concluded that heat transfer across the screen meshes was dependent upon barrier thermal conductivity and that the capillary screen meshes were impervious to natural convection currents.

14. SUBJECT TERMS

orbital cryogenic fluid management, cryogenic liquid acquisition devices, convective heat passage through capillary screen meshes

15. NUMBER OF PAGES

40

16. PRICE CODE

17. SECURITY CLASSIFICATION OF REPORT	18. SECURITY CLASSIFICATION OF THIS PAGE	19. SECURITY CLASSIFICATION OF ABSTRACT	20. LIMITATION OF ABSTRACT
Unclassified	Unclassified	Unclassified	Unlimited

National Aeronautics and
Space Administration
IS20
George C. Marshall Space Flight Center
Marshall Space Flight Center, Alabama
35812